Front. Phys., 2011, 6(2): 162–176
DOI 10.1007/s11467-011-0174-3

REVIEW ARTICLE

Density functional theory calculations of the metal-doped carbon nanostructures as hydrogen storage systems under electric fields: A review

Zhi-wei ZHANG (张志伟), **Jian-chen LI** (李建忱)†, **Qing JIANG** (蒋青)*

Key Laboratory of Automobile Materials, Ministry of Education, and School of Materials Science and Engineering, Jilin University, Changchun 130022, China

*E-mail: †ljc@jlu.edu.cn, *jiangq@jlu.edu.cn*

Received June 29, 2010; accepted March 10, 2011

This review covers structural, electronic, and hydrogen storage properties of carbon-based materials with doped metals under electric fields with different orientations and intensities, which are determined by density functional theory (DFT) simulations. The special application case is considered in investigating variations of electronic structures, binding, and hydrogen storage properties. External fields that are often met in practical applications lead to changes of the above properties.

Keywords hydrogen storage materials, electric field, first-principles calculations

PACS numbers 84.60.Ve, 87.50.Rr, 31.15.Ar

Contents

1 Introduction

Globally, the utilization of fossil fuels has been causing serious air pollution and enormous release of greenhouse gas. Also, the reserves of unrenewable fossil fuels are limited in the Earth. Therefore, searching for an abundant, renewable, and especially clean, alternative energy resource is urgent for the mankind. Hydrogen is being considered as a promising alternative fuel because of its efficiency, abundance and environmental friendliness [1, 2]. Hydrogen is a promising clean energy carrier and has been attracting much interest from scientific communities, governments and industries [3]. However, a hydrogen economy has not come into being. One of the primary technical challenges is the lack of economic, effective and safe hydrogen storage mediums. The current methods of storing hydrogen as compressed gas or in the liquid form do not meet the industrial requirements because the energy densities are much lower than that in gasoline. Moreover, there are issues of safety and cost involved in compressing hydrogen under high pressure or liquefying it at cryogenic temperatures. Although storage of hydrogen in solid state materials offers an alternative, there are no such materials meeting the requirements at present.

During the last one or two decades, there has been intense research on hydrogen storage materials. According to the actual knowledge, solid state storages can be divided into two categories. The first one is physisorption on surfaces of solids. In this process, H_2 molecules are bonded to a surface by van der Waals forces. The second is characterized by dissociation of the hydrogen molecules, and atomic hydrogen can be chemisorbed on the surface by forming a covalent bond. Chemisorbed hydrogen has a binding energy of more than 2–3 eV, compared to approximately 0.1 eV for physisorbed hydrogen [4]. None of the two different storage solid state methods proposed so far fulfils all requisites for a large scale

application in the field of land transports.

Storage capacity and binding strength represent two most basic parameters to characterize hydrogen storage materials. We need higher former and a moderate latter between the physisorbed and the chemisorbed states [5, 6] where both storage and release of H_2 are necessary. Thus, the US Department of Energy (DOE) proposed goals, such as that the H_2 capacity should exceed 6.0 wt%, and that the adsorption energy E_{ad} should be between -0.20 and -0.70 eV/H_2 at room temperature [7, 8]. Furthermore, the storage materials should be able to reversibly adsorb/desorb H_2 in the temperature range of -20°C to 50°C under moderate pressures (maximum 100 atm).

To achieve this goal, hydrogen storage media should only be considered among systems composed of light elements. Carbon nanostructures materials with chemical stability and optimal density, including carbon nanotubes (CNT) [9–14], fullerenes [6, 15, 16], and graphene [10, 17], are the most promising hydrogen storage mediums. Among these carbon materials, the properties of the recently discovered graphene represent a quandary. Although its super-high strength and unusual electronic properties are attractive for a hydrogen storage medium [18–20], its flat surfaces may adsorb fewer H_2 than those with curvatures, such as nanotubes, since the curvature of a surface and related higher number of carbon atoms interact with more H_2 molecules [21]. Because relatively large graphene sheets, up to 100 microns in size, have been successfully synthesized [22], the hydrogen storage behavior of graphene is actively being studied and compared to those of CNT and fullerenes [23–25]. The advantages of carbon nanostructures are: i) a large surface for H_2 adsorption, ii) economical and scalable production [26], and iii) the strongest material ever measured [27]. However, pristine carbon nanostructures are chemically too inert to act as a possible hydrogen storage medium [28]. Experimental studies have shown that, at room temperature and under ambient pressure, the hydrogen storage capacity (HSC) and the E_{ad} value of H_2 with pristine CNT are both too small, which may not exceed 1 wt% and -0.030 eV, respectively [2, 13, 29]. Attempts have thus been made to improve the binding of H_2 with functionalized carbon nanostructures. One possible approach to increase their chemical activity is to modify the nanostructures by doping or substitution of alkali metals (AM) [6, 30–32], transition metals (TM) [33, 34], rare earth metals (RE) [35], etc., which improves their HSC [16, 31–33, 35–39].

Previous experimental and theoretical studies have shown that doping TM atoms or AM atoms on carbon-based material can appreciably enhance the adsorption energy of H_2 [10, 32, 40–46]. However, there are also many problems about the hydrogen storage mechanism and the processes that limit the application and development of hydrogen storage materials. Yildirim and Ciraci, for example, studied a Ti-decorated CNT surface and found that up to 8 wt% of hydrogen could be absorbed on the Ti-doped CNT if the Ti atoms could be uniformly coated on the nanotube surface. Sun *et al.*, however, showed that Ti prefers to cluster on fullerene C_{60} surfaces and is thus not effective in increasing the binding of H_2 to the Ti-doped fullerene [47]. They further studied a Li-dispersed fullerene system and found that Li atoms prefer to stay as atoms on these surfaces because the binding energy between Li and C_{60} is slightly higher than the cohesive energy of Li clustering. H_2 bind to the Li on the CNT surface with a binding energy of 0.075 eV/H_2 and a capability of 13 wt% [6]. Cabria *et al.* studied the interaction of H_2 with Li-doped graphene and CNT using the first principles density functional method and found that the E_{ad} value of H_2 with the Li-doped system was greater than that with a pure carbon system [10]. In fact, the Li-doping surface modification technique becomes a novel research focus in hydrogen storage studies recently. Huang *et al.* reported that a Li-decorated benzene molecule could be used as high-capacity hydrogen storage medium near room temperature from their first principles calculations [48]. Some theoretical and experimental studies have also found that doping the metal-organic frameworks (MOFs) with Li is a good strategy to enhance the hydrogen storage performance [49–52].

Aluminum hydrides as potential hydrogen storage materials have been examined due to their potentially large HSC of 10 wt% and kinetic stability [53]. However, the large amount of hydrogen desorption energy is a critical obstacle for practical applications. Accordingly, methods to reduce the interaction between H and Al have been explored. Several groups have investigated the use of carbon materials as possible catalysts for hydrogenation and dehydrogenation of $NaAlH_4$, and the samples were almost exclusively ball milled [54, 55]. These experimental observations demonstrated that carbon materials as a catalyst render $NaAlH_4$ reversible and improve hydrogen sorption behaviors. Furthermore, Berseth *et al.* not only found that carbon nanostructures can be used as catalysts for hydrogen uptake and release in metal hydrides, but also provided an unambiguous understanding how the catalysts work [56]. Situations involving the electron being transferred elsewhere than the AlH_4 unit will result in weakening of the Al–H bond and lowering of the hydrogen desorption energy. This has led to optimism that alanates may be suitable materials for hydrogen storage. In addition, graphene appears to be promising for such a purpose because of its strong interaction between the H_2 molecule and the graphene along with a large surface area for adsorption.

External fields, which are often met in practical applications, could induce further changes in these materials, and yield substantial alternations in geometry, binding

energies, vibrational spectra, and electronic properties [22, 57–64]. Experimentally, angle-resolved photoemission results showed that an electric field is associated with the charge transfer from dopants to the carbon atoms in a K-doped graphene bilayer [61]. Newly developed graphene layers have also exhibited a pronounced response to a perpendicular electric field due to its high electronic behavior [22]. For instance, the electronic gap of a graphene bilayer can be controlled externally by applying a gap tunable by the electric field [64]. Theoretically, the superimposition of an external electric field is predominantly done with the density functional theory (DFT) method [65–68]. For example, the generalized gradient approximation (GGA) functional has computationally studied the electric field enhanced hydrogen adsorption phenomena on a nano-scale BN sheet, where the calculated E_{ad} drops dramatically from -0.07 to -0.48 eV/H_2 in the presence of a 0.050 au field [69]. In addition, a very recent work revealed that quaterthiophene molecules are strongly polarizable by electric fields along the long direction of the molecule, and such a polarization changes the Highest Occupied Molecular Orbital (HOMO) and the Lowest Unoccupied Molecular Orbital (LUMO) levels and can provide local attractors for holes and electrons [70]. Thus, application of an electric field to a polarizable substrate provides a novel way to store hydrogen. Once the applied electric field is removed, the stored H_2 molecules can be easily released, making thus storage reversible with fast kinetics. In addition, materials with rich low-coordinated nonmetal anions are highly polarizable and can serve as a guide in the design of new hydrogen storage materials.

As stated above, DFT has nowadays become one of the most popular and successful quantum mechanical approaches to matters, which offers distinct advantages in electronic structure determinations [71]. In the simulation, the simulator builds a model of a real system and explores its properties. The model is a mathematical one and the exploration is done on a computer, and in many ways simulation studies share the same mentality as experimental ones. However, simulations allow absolute control over experimental parameters and access to outcomes in details. These strengths have been exploited for the last fifty years since the introduction of computation algorithms has allowed one to calculate the properties of materials based on first-principles outlined in Schrödinger equation without free parameters. For example, experimental study of size-dependent catalytic behaviors is challenging due to the difficulties associated with the preparation of uniform samples with varying dimensions. In this case, computer simulation, in particular the DFT, is gaining importance. The foundation of DFT is two theorems proposed by Hohenberg and Kohn [72], which states that the total energy of a system with interacting electrons is a unique functional of the electronic density, and that the ground state electron density determines the ground state total energy. Now, many softwares, such as MS modeling [73], include DFT calculation code, like CASTEP and DMol^3 codes [74, 75]. CASTEP is a program based on total energy plane-wave pseudopotential methods, which employs DFT to simulate the properties of solids, interfaces, and surfaces for a wide range of material classes [76]. Owing to its unique approach to electrostatics, DMol^3 has long been one of the fastest methods for molecular DFT calculations and can quickly perform structure optimizations of molecular systems. Within DFT it is possible to study hydrogen storage material in details, and moreover, to build up theoretical databases, from which general trends and concepts can be extracted.

In this review, we will focus on how first-principles DFT method and an external electric field can be applied to calculating different metal elements doping on carbon-based hydrogen storage systems in Sections 2 to 5. Section 6 summarizes the main contributions and limitations of these simulation works with suggestions for future directions in extending the developed knowledge and associated approaches. All DFT calculations were performed with the DMol^3 code [74, 77]. The "Electric_Field" keyword in the DMol^3 code allows us to specify the direction and intensity of an electric field.

2 Hydrogen storage based on alkali metals doped carbon-based materials

2.1 Li-doped single-walled carbon nanotubes

Recently, many attempts have been made to increase the E_{ad} value of H_2 on functionalized carbon materials such as on Li-doped CNT. New AM doped pillared carbon materials have been designed to achieve practical reversible hydrogen storage for transportation [10, 12, 13, 32, 40–42]. Theoretically, Chen *et al.* discussed the adsorption of H_2 on bare nanotube and Li-doped one, and found that E_{ad} is -0.025 eV and -0.18 eV, respectively [13]. Cabria *et al.* studied the interaction of H_2 with Li-doped (4, 4) CNT, and showed larger E_{ad} of -0.173 eV [10]. Wu *et al.* performed first-principles calculations with GGA for exchange and correlation functional, and also proved that the E_{ad} value of H_2 on Li-doped (8, 0) CNT is increased to -0.162 eV [12]. Experimentally, although earlier experiments suggest 20 wt% H_2 for Li-doped nanotubes in moderate temperature [40], subsequent experiments showed that H_2 wt% is not so high. Yang *et al.* measured H_2 wt% of Li-doped CNT by thermogravimetric analyzer and found that the hydrogen uptake is only 2.5 wt% [41]. Pinkerton *et al.* did not detect any evidence of H_2 adsorption by Li doped CNT under their experimental condition [42]. These results suggest that the adsorption

energy of H_2 on Li doped CNT increases compared with that on the undoped nanotubes. However, the amount is still below what is required at room temperature. It is interesting to point out that a bare Li^+ can hold at least six H_2 with the largest E_{ad} of -0.253 eV which is much larger than that on the Li-doped nanotubes [78]. It is found that the weaker binding of H_2 on Li-doped CNT is due to the much reduced localized charge of Li adsorbed on the nanotube. Recently, Chen *et al.* found that binding of H_2 on Li-doped nanotube can be enhanced when there are C_{60} molecules encapsulated inside the tube [13]. Their analysis showed that the electron acquirement of C_{60} molecules from the nanotube makes the tube positively charged, which helps more charge transfer from the Li atom to the nanotube. As a result, the Li atom has more localized charges and the adsorption of H_2 is strengthened. This result indicates that when Li-doped nanotube is positively charged, adsorption of H_2 on it can be enhanced. In order to find how the charge of Li-doped CNT affects the adsorption energy of H_2, Ni *et al.* used first-principles DFT to study the hydrogen adsorption on Li-doped charged CNT by changing the electron number of these systems and discussed the largest number of H_2 adsorbed by the Li-doped charged CNT [79]. The adsorption of H_2 on positively charged Li-doped CNT is enhanced compared with that on uncharged systems. As the charge of the Li-doped CNT increases, the E_{ad} value of H_2 increases with the largest E_{ad} being -0.26 eV. The reason for the increase in H_2 adsorption energy is that the positively charged tube improves the charge transfer from the Li atom to the tube and makes the Li atom more ionized, which strengthens the polarization interaction between H_2 and Li atom.

Recently, Liu *et al.* found that the electric fields can be imposed to realize the ideal case for H_2 storage: Increasing the bonding in the adsorption process and decreasing it during the desorption one. Compared with other approaches, the fields have many advantages for practical applications, such as being clean, easily acquirable, and adjustable in both direction and intensity. In recent published works, an 8-Li-doped CNT (the Li_8/CNT system) has been established as a hydrogen storage material [30]. The calculation demonstrated that at most 64 H_2 molecules can be adsorbed, which renders a 13.45 wt% of HSC. Therefore, the multiple Li doped CNT is employed as a model material to look into the influence of electric fields on H_2 binding strength. It is noteworthy that most previous studies addressed the problem of bonding enhancement but failed to address the problem of how to decrease the binding during the desorption process. In fact, the binding will weaken if the charges transfer in a contrary direction, i.e., from the nanostructures to the dopants. This can be readily accomplished by simply changing the direction of the superimposed electric fields. Several electric fields with different directions and intensities are applied to the relaxed Li_8/CNT storage materials.

First, let us consider the results obtained at F=0. For the relaxed Li_8/CNT, the Li–C atomic distance l_{Li-C}=1.48 Å with a relatively strong binding of 1.82 eV/atom. Charges transfer from the dopants to the CNT in terms of the Mulliken analysis: Li presents a net charge of $+0.291$ e, while the neighboring C atoms present negative ones of -0.088 e and -0.013 e. These results verify the stability of 8-Li-doped models. After full relaxation, H_2 is parallel to CNT at the Atop site with $E_{ad} = -0.15$ eV/H_2. In contrast, the Bridge site is more preferable than the rest. The storage materials expand slightly after H_2 is adsorbed in terms of the l_{Li-C} values.

The authors address the effect of F on E_{ad} values for the H_2/Li_8/CNT. E_{ad} values at the Bridge site decrease dramatically to -0.58 eV/H_2 under F=+0.010 a. u.. This is almost doubled in comparison with $E_{ad} = -0.30$ eV/H_2 at $F = 0.000$ a. u.. Furthermore, it is even fivefold lower than $E_{ad} = -0.10$ eV/H_2 on a pure CNT. The geometry of CNT varies severely under the field, with the shape of the cross section changing from circular to elliptical. When d_{Li-H} values from different sites are observed, there is a sequence of Bridge < Middle < Atop, which is consistent with the sequence of their corresponding E_{ad} values. Thus, the binding strength between the H_2 and Li is inversely proportional to their corresponding d values, even though in the presence of fields. In contrast, the field seems to have no obvious contribution to E_{ad} values for H_2/Li/CNT and H_2/CNT systems. This may be due to the weak spin variation around the nanotube induced by only one metallic atom or even lack of any metallic atom. In fact, only a 2.36% charge variation can be detected under the fields for the Li atom in the Li/CNT system.

To understand the reason why the binding can be enhanced under F=+0.010 a. u., the Mulliken charge analysis is carried out for the Bridge site. On the one hand, the charge carried by each Li increases considerably from $+0.291$ e to $+0.423$ e for the unadsorbed system since the electrons will move downward from Li to the carbon ring under a positive field. On the other hand, the charges of the surrounding six C atoms decrease from -0.088 e to -0.118 e, or from -0.014 e to -0.048 e. Therefore, the positive field gives rise to the enhancement of charge transfer from Li to C, i.e., further ionization [10], which increases the H_2 sorption. After adsorption, the H_2 loses 0.187 e while Li obtains 0.220 e charges, whereas small changes can be found in C atoms.

Obviously, opposite binding trends might be achieved if negative fields are employed. Compared with the data without fields, all the binding values are weakened under $F = -0.010$ a. u.. All their l_{Li-H} values increase after the introduction of the field. The CNT is severely com-

pressed along the direction of the field. It is interesting to find that the C atoms are no longer anions, but carry positive charges with values that range from +0.011 e to +0.030 e. Since both Li dopants and the carbon rings are positive under $F = -0.010$ a. u., it is obviously not advantageous for the H_2 storage. However, this should be a good result for desorption process as it weakens the binding between the H_2 and the storage material.

Figure 1 provides the field intensity dependent results for the H_2/Li_8/CNT system at the Bridge site. The binding strength is enhanced (or weakened) as the intensity of the positive (or negative) field increases. Although the trend is that as the field increases the binding becomes stronger, it is apparent that the F value cannot be infinitely large. In addition to the energy consumption, as F reaches 0.030 a.u. the entire system was severely compressed along the direction of the field, and the excellent electronic properties of the Li-doped CNT would be degraded. Note that in this figure, a plateau can be seen around -0.005 a. u. $< F <$ +0.002 a. u. in the $E_{ad}(F)$ curve. Mulliken charge analysis shows that the weak intensity cannot effectively "drive" the charge transfer within the system. On the other hand, although larger electronic redistribution occurs under $F = -0.005$ a. u., it is interesting to find that some C atoms carry negative charges, whereas the other C atoms carry positive ones. This is quite different from the case corresponding to $F = -0.010$ a. u., namely, that all C atoms in the hexagon are fully positive, and thus render a significantly decrease in the H_2 binding strength. What is also different from those under F=+0.010 a. u. is that all the C atoms are negative, and thus a strong heteropolar bonding takes form between CNT and the Li dopant. Therefore, $F = -0.005$ a. u. here seems as a "transition state" during the charge redistribution process, and the influence of the field is "counteracted" by their own negative and positive C atoms to some extent. This is

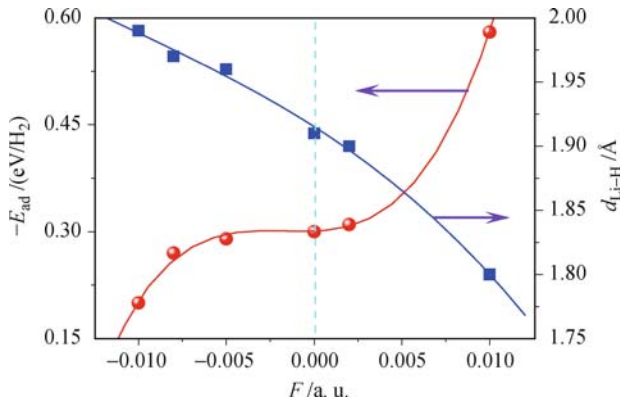

Fig. 1 Influences induced by the intensity of fields for the Bridge site of the H_2/Li_8/CNT system. The plot shows the $-E_{ad}$ (*sphere line*) and d_{Li-H} (*square line*) values with respect to F where the discrete data are fitted by a third-order exponential function. When F=0.000 a. u., the $-E_{ad}$ value of 0.30 eV/H_2 and d_{Li-H} value of 1.91 Å are selected as references. Reproduced with permission from Ref. [66], Copyright © 2009 Royal Society of Chemistry.

presumably the reason why the E_{ad} value is so "insensitive" to the F values in this range. Note that this insensitivity is relevant for practical applications since any small unexpected field fluctuation will not cause a state change.

In addition to energy, some regularity induced by electric fields can also be observed in the geometric parameters for the H_2/Li_8/CNT systems. As shown in Fig. 1, l_{Li-H}=1.80, 1.90, 1.91, 1.96, 1.97, and 1.99 Å when F=+0.010, +0.002, 0.000, −0.005, −0.008, and −0.010 a. u., respectively. Similarly, l_{Li-C}, and D_x increase, while l_{H-H} and D_y drop when stronger intensity is introduced into the storage materials. This suggests that in addition to the direction, the intensity of the fields is also an efficient parameter in adjusting the hydrogen storage.

Finally, to further understand the electronic hybridizations, the DOS plots are determined and shown in Fig. 2 for the H_2/Li_8/CNT system. When F=0.000 a. u., on one hand, the main peak of Li-2s located at −9.40 eV hybridizes with the σ bonding of the H_2 molecule in the lower energy range, see Fig. 2(a). On the other hand, the bands of Li interact with those of C at the higher energy range, where a sharp peak can be observed around −7.75 eV. This suggests that Li acts as a "bridge" in this reaction, which interacts with the H_2 molecule and the CNT simultaneously. It is known that all structures of CNT are made up of the sp^2 orbital of C atoms. After the Li and H_2 adsorptions, this orbital will change from the sp^2 to sp^3-like bonding, although the degree is not as large as that of the hydrogenation [80, 81]. Figure 2(b) shows the bands interactions under F=+0.010 a. u., from which it is clear that although the orbitals under F=0.000 and F=+0.010 a. u. are quite similar, the former should be more stable since it has more evident peaks at the lower energy range. Compared with Fig. 2(a), the main peak of Li under fields moves toward the Fermi level and hybridizes with the σ bonding of H_2 at −6.49 eV. Similarly, the π orbital of the CNT varies from −2.06 to −0.90 eV under F=+0.010 a. u., and overlaps with the Li-2s orbital just below the Fermi level. It is noteworthy that the amount of C electrons near the Fermi level (around −5.00∼0 eV) in Fig. 2(a) is much smaller than that in Fig. 2(b), whereas larger than that under $F = -0.010$ a. u. in Fig. 2(c). These results may be attributed to the fact that the C atoms obtain charges under the positive fields, whereas lose charges under the negative fields. In Fig. 2(c), the orbitals of H, Li, and C interact tightly with each other within the lower energy range. In comparison with Fig. 2(b), the bands of Li further move to the Fermi level and the sharpest peak hybridizes with H at −0.88 eV. In addition, the π orbital of the CNT hybridizes simultaneously with the s orbitals of H and Li around −1.33 eV. These DOS changes confirm the strong effect of Li dopants in the hydrogen storage systems, even

under electric fields.

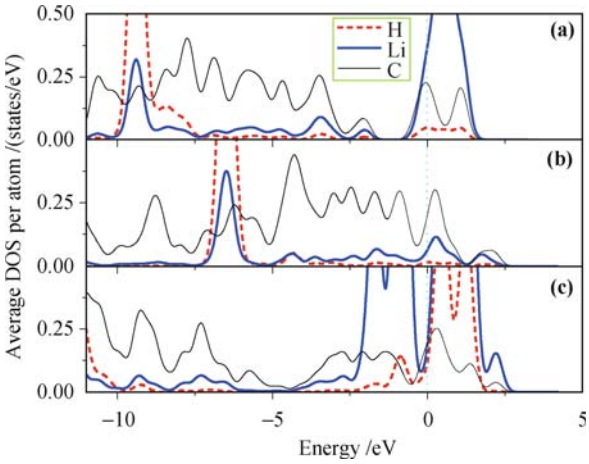

Fig. 2 The DOS plots under different fields. **(a)** F=0.000 a. u., **(b)** F=+0.010 a. u., and **(c)** F = −0.010 a. u. for the H_2/Li_8/CNT system at the Bridge site. Reproduced with permission from Ref. [66], Copyright © 2009 Royal Society of Chemistry.

2.2 Li-doped single-layer and bilayer graphenes

Although the CNT was selected as a prototype in the previous work, it is clear that this idea can be extended to other weak storage systems such as the graphene sheets. A strong binding strength will be detrimental when H_2 release is required [82]. Hence, physisorption and chemisorption of H_2 represent more viable mechanisms for hydrogen storage applications [83]. The main challenge is that the binding between H_2 and graphene is quite weak (merely on the order of −0.10 eV/H_2), which effectively yields a low storage capacity [10, 84, 85]. Therefore, the attainment of moderate adsorption energy has remained a challenge, either due to weak physisorption or, at the other extreme, due to strong chemisorption that renders hydrogen release difficult. More recently, a few novel approaches have been proposed to enhance the storage ability of graphene-based systems. For example, by doping the graphene with Li, the binding strength increased two-fold (E_{ad} = −0.184 eV/H_2) over that of the undoped material. In related work, it was reported that Li atom can be adsorbed on graphene forming a uniform and stable coverage on both sides, which can serve as a high-capacity hydrogen storage medium [24, 38]. A recent report of a novel storage model is noteworthy which comprises of 3D pillared graphene [86]. Although this material was anticipated to reach the volumetric target of DOE, fabrication issues have precluded experimental verification.

In light of the above discussion, Liu *et al.* hypothesize that the imposition of an electric field on Li-doped graphene can be used to control the binding strength during adsorption and desorption. Both single-layer and bilayer graphenes will be chosen as prototypes in these calculations; inspection of the scientific literature fails to reveal prior studies on bilayer graphenes. In this section, Li-doped single-layer and bilayer graphenes are utilized as hydrogen storage models. External electric fields, with different intensities and orientation are superimposed into the relaxed systems.

The E_{ad} value for the H_2/Li/single-layer graphene decreases dramatically to −0.288 eV/H_2 under F=+0.020 a. u.. As mentioned above, GGA predicts that H_2 cannot be stably adsorbed without a field. Therefore, the negative E_{ad} value under +0.020 a. u. further confirms that a positive field can evidently enhance the interactions between H_2 and the Li-doped graphene. Similarly, the E_{ad} value decreases from −0.225 (or −0.219) to −0.288 (or −0.277) eV/H_2 in the case of two (or three) molecules, leading to an approximate 30% binding enhancement. Nevertheless, the $4H_2$/Li/single-layer graphene seems to be "insensitive" to the presence of external fields. To explain this phenomenon, a Hirshfeld charge analysis was carried out for this system, and the results showed that Li carries a +0.191 e charge in the absence of the field. This value only increases to +0.208 e when F=+0.020 a. u.. Now that only a 2.23% charge variation can be detected for each H_2, it is safe to argue that the field indeed has a limited influence on the $4H_2$ system. In contrast, opposite binding trends are observed when F = −0.020 a. u.. The negative field results in a 2.54% to 55.11% binding strength decrease as compared to the cases in the absence of a field. Therefore, the imposition of a negative field is beneficial to the release of H_2.

To understand the above E_{ad} variations induced by the presence of an electric field, Hirshfeld charge analysis was carried out for the H_2/Li/single-layer graphene. These results make physical sense, since the electrons will move downward from Li to the carbon sheet after the superimposition of an upward field. As Li is more positive and graphene is more negative, F=+0.020 a. u. renders an extra dipole moment and thus enhances the hydrogen adsorption. After adsorption, the molecule obtains 0.003 e while Li loses 0.043 e in the absence of a field. This is consistent with the results from a prior study which show that H atoms receiving a charge from Li become negatively charged and the covalent H–H bond becomes polarized [38]. In contrast, H atoms become cations and the charge of Li decreases from +0.417 e to +0.334 e when F=+0.020 a. u.. These results are caused by the downward charge transfer (from H_2 to Li) in the presence of a positive field. In the case when F = −0.020 a. u. field is imposed, the charge Li carried decreases significantly from +0.219 to +0.033. The corresponding charges carried by C are approximately zero, ranging from −0.009 e to +0.007 e. This charge redistribution is evidently attributed to the upward charge transfer induced by a negative field. Since the ionizations of both Li and C have decreased considerably, the hydrogen binding will be weakened, and this is presumably the reason why a negative field facilitates the release of H_2. In contrast to

the cases when F=0.000 a. u. and +0.020 a. u., the ionization might be further degenerated since the influence from C atoms may counteract each other in the graphene sheet.

Similar to the situations in the single-layer systems, Li transfers a portion of its charge to bilayer graphene and thus carries +0.245 e in the absence of a field. BV is also the most preferable site for the H_2/Li/bilayer graphene system. As all H_2 are tilted after full relaxation, one of the two H atoms of each adsorbed H_2 becomes relatively closer to the Li dopant [38]. It is noteworthy that bilayer graphene has a slightly stronger binding strength than that of the single-layer graphene system. Figure 3(a) can be used to explain this phenomenon, in which not only the C atoms in the upper layer, but also those in the lower layer carry negative charges, although the amount is quite small. Since both of these two layers can "adopt" charges, the Li dopant is more ionized on the bilayer graphene. The above results can also be visualized in the plots of electron density differences. As shown in the insets of Fig. 3(a), all carbon atoms in both sheets turn red after doping, indicating that the electron has been enriched in these areas.

On the basis of the above results, it is apparent that charge redistribution occurs in the above system after superimposing an electric field. As shown in Fig. 3(b), the charge carried by Li increases considerably from +0.245 e to +0.449 e under a positive field. Partial electrons move from Li to the neighboring C ring. Interestingly, slight variations (0.001 e to 0.003 e) can be observed in comparison with the C atoms shown in Fig. 3(a). This is presumably because the electrons obtained from Li are not accumulated in this hexagonal ring, but will flow to the remaining C atoms in the same layer and the lower C sheet. Correspondingly, the E_{ad} value for the H_2/Li/bilayer graphene system decreases largely from −0.188 to −0.294 eV/H_2 when F=+0.020 a. u.. Similar binding enhancement can also be observed for the storage models in the case of 2 to 4 H_2 molecules, although the variations are not as significant compared to the one-H_2 system.

In contrast, electrons move upward from C to Li in the presence of a negative field. As shown in Fig. 3(c), the C atoms in the upper layer remain anions but carry fewer

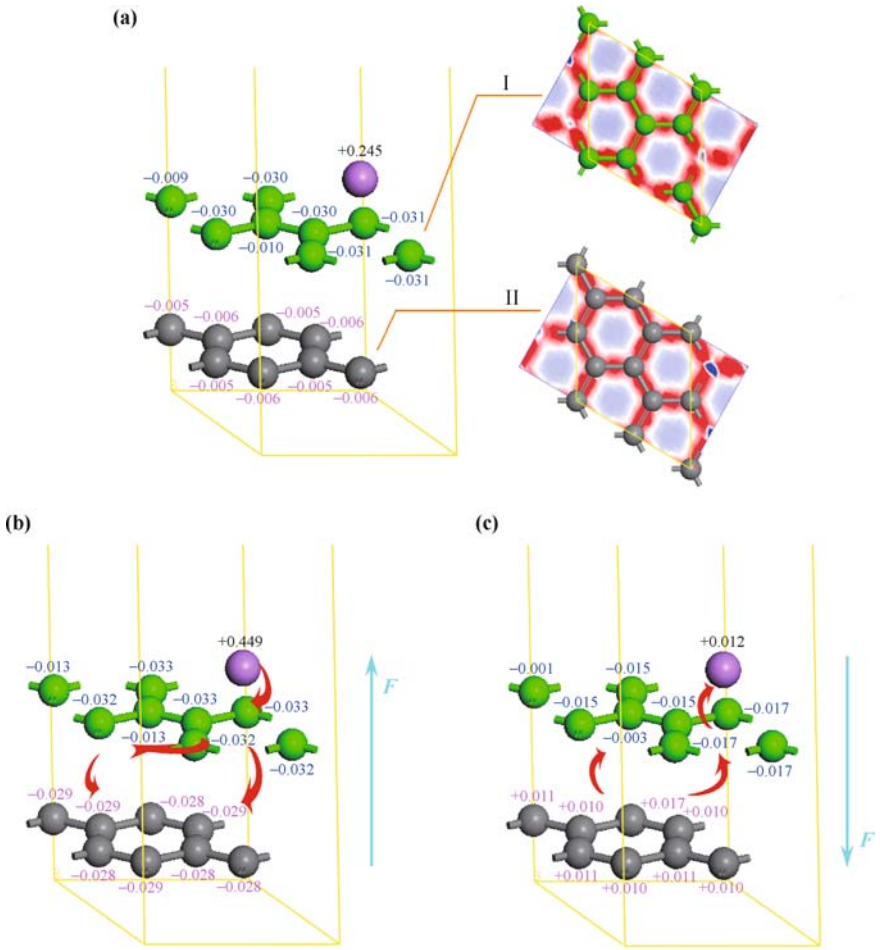

Fig. 3 Hirshfeld charge analysis for the Li-doped bilayer graphene under: **(a)** F=0.000 a. u., **(b)** F=+0.020 a. u., and **(c)** F=−0.020 a. u., where the red arrows indicate the possible charge transfer directions within these systems. In plot (a), insets I and II show the electron density difference for the upper and lower carbon layer, respectively. The red (or blue) region shows the location where the electron density has been enriched (or depleted). Reproduced with permission from Ref. [67], Copyright © 2009, Elsevier.

negative charges when $F = -0.020$ a. u.. Surprisingly, all C atoms in the lower layer become cations. Thus, the two layers may counteract each other and reduce the polar moments of the entire graphene. In addition, it is readily seen that the charge carried by Li turns out to be merely $+0.012\ e$, which is much smaller than $+0.245\ e$ in the absence of field. The negative field can significantly weaken the H_2 adsorption.

From the above discussion, it is concluded that F can be utilized as a switch to control the entire adsorption and desorption in the hydrogen storage systems. After full relaxation, entire systems are elongated even in the presence of upward or downward fields. This agrees with a prior result showing that clusters of particles are expanded along the direction of the field [87]. The rational is that although the opposite electrostatic forces are superimposed, the charge separation occurs, rendering an elongation of the unconstrained system. Therefore, both the direction and the intensity of F play important roles in hydrogen storage systems. In addition, this idea may also be utilized to solve the releasing problem for the extremely strong binding systems, such as the Ti-doped nanostructures and the Metal Organic Frameworks. In summary, the present work clearly demonstrates that the electric fields can be used as a useful reversible switch to control the adsorption and desorption processes of H_2.

3 Hydrogen storage based on group-III metals doped carbon-based materials

AlH_3 and related aluminum hydrides as hydrogen storage materials have recently become the focus of renewed interest because of their potentially large HSC of ∼10 wt% [53, 88]. These materials are thermodynamically unstable in ambient, but are kinetically stable without much loss of hydrogen for years. Despite these excellent properties, extremely high pressure (exceeding 2.5 GPa) is required for H_2 adsorption. While these hydrides possess a small negative enthalpy of formation [88], for practical applications the large H_2 desorption energy proves impractical. The origin of this energy barrier lies in the rather strong mixed ionic and covalent bonds, formed between Al and H. Thus it is essential to reduce significantly the desorption energy.

There appears another way for Al atoms to store hydrogen, i.e., to further decrease the interaction between Al and H. In this way, the weak chemisorption can be changed into strong physisorption. For hydrogen storage through physisorption, strong interaction between the H_2 molecule and the surfaces along with a large surface area for adsorption are required. The unique characteristics of graphene and Al for hydrogen storage lead to an investigation of the properties of Al doped graphene as a possible hydrogen storage candidate. It would be intriguing to understand the interaction between graphene, Al and H. In this section, DFT is employed to study H_2 adsorption on defected graphene with Al atoms. The favorite adsorption configurations of Al atoms on single side and on both sides of a graphene layer are determined. Al-doped graphene where one Al atom replaces one C atom of a graphene layer was reported as a promising hydrogen storage material at room temperature with HSC of 5.13 wt% [39]. It was found that Al alters the electronic structure of both the graphene layer and the H_2 molecules. The underlying mechanism of HSC enhancement is caused by the overlapping bands of the H_2 with those of Al and C.

Al adsorbed at the hollow site has the lowest energy and is therefore the favorite adsorption configuration with a binding energy of −0.824 eV, and the distance between Al and the graphene layer d_1 is about 2.079 Å. Note that the other two C atoms in the simulation cell contribute the rest of the electron charge to the negative C atoms. Therefore, the long distance of Al–Al, the relative strong bonding between the Al atom and the graphene layer, and the Coulomb repulsion between the Al atoms prevent metal aggregation. The diffusion behavior of an Al atom on graphene was studied by the transition search (TS) method in order to obtain the diffusion barrier. It is found that the classical barrier for surface diffusion is 0.104 eV. While in actual diffusion, the Al–Al distance would be shortened, and the repulsive Coulomb interaction among positively charged Al atoms would increase, leading to a significant increase of the diffusion barrier, which will prevent aggregation of adsorbed Al atoms on graphene.

Two Al atoms are positioned on two shoulder-by-shoulder carbon hexagons but on opposite sides of the graphene layer. The repulsive Coulomb interaction between the positively charged Al atoms on the upper and lower parts of the graphene plane is screened by the negative charge on the C atoms. The graphene layer is more negatively charged as compared to the previous single Al atom case, while the adsorbed Al atoms are more positively charged. It leads to a stronger binding energy for the Al atoms on the graphene. In addition, $d_1 \approx 2.138$ Å, which is slightly larger as compared to the case of single side adsorption which is counter intuitive. The reason is that the small increase of d_1 is a result of the Coulomb repulsion between the two positively charged Al atoms located above and below the graphene layer, which is screened by the charged graphene.

For the case of H_2 adsorption on Al that is adsorbed on both sides of graphene, the situations of one, two and three H_2 molecules adsorbed on each side of graphene are quite similar to the case of adsorption on a single side of graphene. Four H_2 are adsorbed on each side. Two of them take the center sites of equilateral triangles, and the other two are located on the bridge sites of the two

Al atoms. However, the four H_2 molecules are in two different planes with distances to the graphene layer being 2.672 and 4.675 Å. The distances of the four H_2 to the Al atom are respectively 2.444, 2.531, 2.918, and 2.947 Å. The average E_{ad} is -0.209 eV/H_2. If the amount of H_2 is further increased, the two H_2 in the center sites of the equilateral triangles will hop to the bridge sites of the two Al atoms while keeping the two-layer structure. Therefore, each Al atom can adsorb a maximum of six H_2 due to the two-layer adsorption structure, and each Al atom has six nearest Al atoms with each adsorbed H_2 shared by two Al atoms. All H_2 are located at the bridge sites of Al–Al and are arranged into two layers on each side of graphene. Note that the adsorption of H_2 on both sides of graphene will automatically change the sites of adsorbed Al atoms from the center site of the carbon hexagon to nearly the bridge site of the C–C bond. The different locations of the Al atoms in the presence of adsorbed H_2 for single side and both sides of graphene is a consequence of: i) the different charges of Al atoms adsorbed on one side of graphene and on both sides of graphene, and ii) the different amount of adsorbed H_2 molecules. Therefore, HSC is up to 13.79 wt% with an average $E_{ad} = -0.193$ eV/H_2. Note that the obtained HSC is in excess of 6 wt%, surpassing DOE's target, and the obtained E_{ad} is almost within the required range of -0.2 to -0.6 eV/H_2 [89].

For practical purpose, E_{ad} is required to be a weak function of the adsorption coverage X of H_2 molecules on graphene, so that the adsorbed H_2 can be desorbed to almost zero X. E_{ad} is about -0.2 eV/H_2 and X has only a weak effect on E_{ad} as shown in Fig. 4 where E_{ad} (X) varies within 15%. Note that E_{ad} is the lowest when 4 H_2 were adsorbed, because adsorption is strongest when H_2 are located on the center sites of equilateral triangles formed by the adsorbed Al atoms. It was confirmed that one H_2 was first adsorbed at the center sites of the equilateral triangles. Due to the interaction between the H_2, the adsorption with 2 H_2 on each side on the center sites of equilateral triangles comes to a maximum.

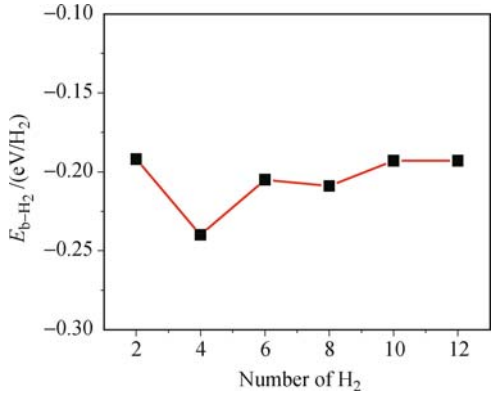

Fig. 4 X dependent average adsorption energy $E_{b-H_2}(X)$ of H_2 on graphene with Al adsorbed on both sides of graphene. Reproduced with permission from Ref. [34], Copyright © 2010 American Physical Society.

When 12 H_2 molecules are adsorbed on both sides of a 2×2×1 supercell of graphene, H_2 on each side of graphene will be arranged into two layers. The distances of each layer to the graphene surface are respectively about 2.5 and 5.0 Å, while d_1 is about 2.2 Å. As discussed above, the E_{ad} for adsorption on both sides of graphene is larger than that for single side adsorption. At the same time, the Al atoms are more positively charged, and the C atoms are more negatively charged when the Al atoms are adsorbed on both sides of graphene. Thus, when Al is adsorbed on both sides of graphene, the graphene layer has a larger capacity for H_2 storage. However, due to the limited space between the Al atoms and the repulsive interaction between the adsorbed H_2 molecules, some adsorbed H_2 move upwards over the Al atoms. This is also the reason why H_2 can form a two-layer arrangement in the case of Al adsorbed on both sides of graphene and only a single H_2 layer is found for the corresponding single side system.

To test the stability of the hydrogen storage system, *ab initio* molecular dynamics (MD) simulations were performed on a 12H_2-Al-graphene system. It was found that only the outer 2 H_2 molecules are escaping from each side of the graphene layer, because they are more weakly bound than the other H_2. For example, the first H_2 that is released has a binding energy of -0.129 eV. In this case, HSC = 9.64 wt%, which is still much higher than DOE's target. This is even the case in the absence of external pressure, and it is thus possible to release H_2 molecules without removing the Al atoms. In addition, the release of H_2 molecules can be further prevented by decreasing the temperature or increasing the pressure of storage to increase its HSC.

To investigate the effect of the concentration of adsorbed Al atoms on its HSC, a 4× 4×1 graphene supercell with one Al atom on the center site of the carbon hexagon above and below the graphene layer was considered. It is found that each Al atom can maximally adsorb 6 H_2 with average $E_{ad} = -0.172$ eV/H_2, resulting in a HSC of 5.19 wt%. The adsorption configuration is shown in Fig. 5. Note that the HSC is much lower than the 13.79 wt% that they found for the 2×2×1 supercell system. In the case of H_2 adsorbed in the 2×2×1 system, H_2 are adsorbed on the bridge sites of Al–Al and are arranged into a two layer configuration. Therefore, each adsorbed H_2 interacts with the nearest two Al atoms. In the 4×4×1 system, which corresponds to a lower density of adsorbed Al, the distance between the two Al atoms is as long as 9.84 Å. Thus, each H_2 interacts with one Al atom and the graphene layer, and there is more space available for the adsorbed H_2 that are located in a single layer. The corresponding E_{ad} also decrease slightly as the Al–Al distance increases. For single and two H_2 adsorbed on a 4×4×1 supercell, E_{ad} are -0.169 and -0.178

eV/H_2. In the case of a 2×2×1 supercell, E_{ad} are −0.182 and −0.227 eV/H_2, respectively.

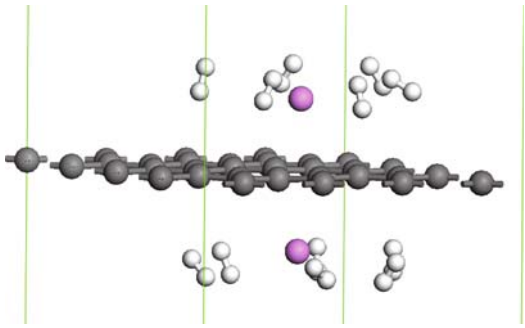

Fig. 5 The configuration of H_2 molecules adsorbed in a 4×4×1 supercell system. Reproduced with permission from Ref. [34], Copyright © 2010 American Physical Society.

In practical applications, it is desirable to know the exact charge status of the hydrogen storage material. From it we can obtain information whether the hydrogen storage material is fully charged or the adsorbed H_2 are completely released. The charge exchanged with the graphene layer can be determined by the conductivity of the graphene layer, which is strongly determined by the DOS at the Fermi level [90, 91]. The X-dependence of the latter quantity is given in Fig. 6. The result shows that the DOS at the Fermi level decreases as X increases and this dependence weakened at high X.

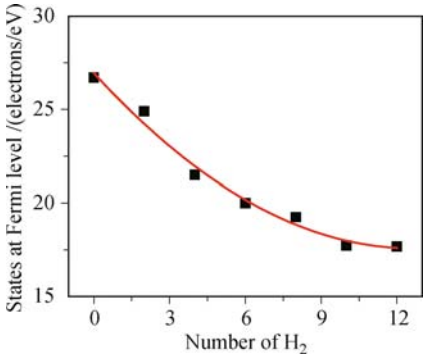

Fig. 6 X dependent number of band states at the Fermi level. Reproduced with permission from Ref. [34], Copyright © 2010 American Physical Society.

4 Hydrogen storage based on transition metals doped carbon-based materials

TM atoms, such as Ti, Pt and Pd, can also bind multiple H_2 molecules [45]. A single Ti atom adsorbed on a zigzag CNT can strongly bind up to four H_2 molecules corresponding to 8 wt% of HSC [43]. And Ti coated buckyballs have a storage density up to 8.77 wt% and desirable E_{ad} value for reversible use under moderate pressure and temperature [92]. It was reported that a single Ti atom adsorbed on the carbon fullerenes and nanotubes could strongly bind up to four H_2 molecules with E_{ad} from −0.50 to −0.10 eV [43]. The favorable H_2 binding to TM results from Kubas-type interactions between the metal and H_2 [43, 93−98], which are much stronger than static Coulomb interactions [6, 16, 32, 38, 86]. TM-decorated materials have H_2-binding strength of as high as 0.4 eV via the hybridization of TM d–H_2 σ and σ^* states, which form the donation and the back-donation channel, respectively [99]. However, a major problem for the metal dispersed on carbon nanostructures is the clustering of metal adatoms due to their large cohesive energies [6, 47]. This clustering tendency must be overcome to maintain a high HSC at a stable level during hydrogen adsorption and desorption processes. In other words, it is necessary to find a way to avoid metal clustering on the surfaces. For example, clustering tendency of the Ti atoms on the silicon-based fullerene surface can be avoided by doping the fullerene with phosphor atoms. However, HSC decreases to 5.0 wt% [100].

To balance both the energetics and weight percentage, recent efforts have been devoted to the design of new materials with exposed metal sites following the mechanisms proposed by Kubas and Niu *et al.* [101, 102]. The Kubas mechanism takes advantage of the unfilled d orbitals of TM atoms where H_2 molecules donate electrons to the unfilled d orbitals and TM atoms back donate the electrons to the H_2 molecules. As a result, H_2 retains its molecular bond, but in a slightly stretched form. The work of Niu *et al.* was focused on metal cations where stretching of the molecular bond of H_2 is caused by charge polarization. The difficulty with the former approach is that TM atoms tend to cluster [43, 47, 93, 103], whereas in the latter the binding energy tends to be lower than the desired value, especially when hydrogen coverage increases [6, 104].

Recently, Bhattacharya *et al.* found that TM-doped defected graphene sheet with periodic repetition of a C atom vacancy can be used as a promising system for hydrogen storage [105]. The TM atoms adsorbed above and below the defected site are found to have a strong bonding to the graphene sheet, thereby circumventing the problem of TM clustering, which is the main impediment for efficient hydrogen storage in nanostructure systems. Thus, the increased binding energy of metals in the case of defected carbon nanostructures may prevent metal clustering on surfaces. B doping is also a practical and feasible way to alter and adjust the binding configurations and the electronic properties of carbon-based materials based on the results of the studies that carbon structure substituted by B shows enhanced hydrogen adsorption performance [106, 107]. In addition, metal adsorption has been studied intensively to enhance the HSC of carbon-based material [38, 39]. Park *et al.* found that Ti atoms are well dispersed on B-substituted graphene because clustering of metal atoms is hindered by the repulsive Coulomb interaction between metal adatoms and the strong bonding force between dispersed metal

atoms and B-substituted graphene [108]. In addition, Ti can bind to eight H_2 molecules on the double side of B-substituted graphene. This allows a high hydrogen storage capacity of as much as 7.9 wt%, which can certainly satisfy the target of the DOE. The dispersed Ti changes the electronic structure of the graphene and H_2. This causes DOS of H_2 to interact with the Ti dispersed on graphene. From these results, it can be inferred that Ti can enhance HSC.

5 Hydrogen storage based on rare earth metals doped carbon-based materials

Previous studies [40] have shown that intercalated AM in CNT would significantly enhance the hydrogen storage. However, the corresponding E_{ad} value is small due to the unstable physisorption state at the ambient condition. When the doping metals are TM, such as the Ni/CNT system, E_{ad} reaches -0.26 eV/H_2 and the adsorption amount of H_2 reaches 10 wt% at the ambient condition. The adsorbed Ni atoms on CNT, however, prefer to assemble forming clusters with about 1 nm in diameters [46]. In the Ti/CNT case, although there is a H_2 storage ability of 7.7 wt% [43], Ti on CNT forms continuous chains with strong Ti–Ti interaction, which reduces the hydrogen binding.

RE doped C_{60} and CNT are other choices for H_2 storage. Suzuk and Deng and their colleagues have studied the geometric and electronic structures of Eu/C_{60}, Sm/C_{60} and Sm/C_{59}, respectively [109, 110]. Wang *et al.* found that Eu prefers to adsorb at the hollow site of the hexagonal ring on the outer surface of the armchair CNT [111]. An important advantage of RE (such as Eu) doping on CNT is that the electronic characteristics originating from the unpaired 4f electrons could serve as electron donors or acceptors to increase E_{ad} for H_2 on CNT. Furthermore, since E_b of RE atom on CNT is large, the clustering problems in metal-decorated nanostructured materials could be overcome. In this section, we examine the hydrogen storage ability of the H_2/Eu/CNT system through investigating the interaction, the bonding characteristics and the adsorption ability with changes of Eu concentration. The results show that the hydrogen storage ability of CNT can be enhanced by doping more Eu atoms.

A single Eu atom prefers to adsorb strongly at H site. The Eu–C distance l_{Eu-C} is 2.48 Å with the binding strength $E_b = 2.01$ eV. The Mulliken charge analysis shows that Eu carries a 1.005 e positive charge, indicating that the Eu atom is ionized and suggesting a possibility for H_2 adsorption due to the polarization mechanism [103]. The interaction between Eu and CNT is primarily ionic due to the charge transfer from Eu-6s to C-2p orbital where the most 6s electrons transfer to π antibonding orbital of the C hexagonal ring. The hybridization essentially occurs among Eu-6s, Eu-5d, and C-2p orbitals. In fact, 4f orbital of Eu also attends the electronic transitions although it is well shielded by the peripheral 6s and 5d ones. After this correction, the charge transfer from Eu to CNT is about 1.767 e, and the Eu atom is divalent for Eu/CNT system.

It is noteworthy that the calculated binding energy for Eu on CNT (2.01 eV) is larger than the calculated cohesive energy of bulk Eu, 1.69 eV (1.86 eV in the experimental value). Since the energy gained from cohesion is much lower than that from binding to CNT, clustering of Eu atoms would not occur on CNT. Figures 7(a) and (b) show the optimized geometries for two aggregated Eu and for individually isolated Eu on CNT. The isolated case is energetically lower by 0.16 eV as compared with the aggregated case, providing ample evidence that Eu atoms do not cluster on CNT. It is suggested that dispersed strong binding sites should exist in absorbents for better metal dispersions, particularly at low metal coverage.

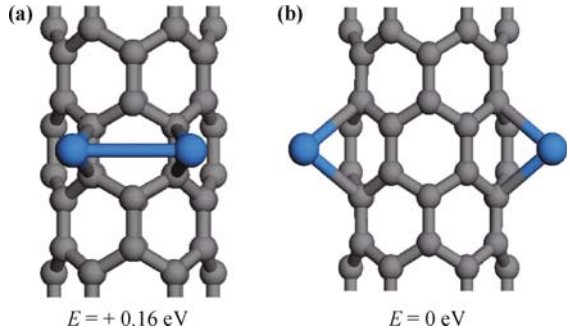

Fig. 7 **(a)** Two Eu atoms aggregated on pristine CNT; **(b)** Two Eu atoms individually attached on pristine CNT. The total energy of the lower energy structure between aggregated and unaggregated structures is set to zero. Reproduced with permission from Ref. [35], Copyright © 2010 American Chemical Society.

The stable Eu adsorbs with a high coverage ratio of 1/8 on (6, 0) CNT without a tendency for clustering. Three Eu atoms are placed on the hollow site of CNT to obtain Eu_3/CNT. After the full relaxation, all three Eu atoms still bind separately on the site without Eu aggregation due to a stronger metal-nanotube interaction with $l_{Eu-C} = 2.54$ Å [112]. The minimum of l_{Eu-Eu} is 7.91 Å, which is almost two times as much as the bulk l_{Eu-Eu} (3.97 Å). Thus, this adsorbate with a coverage ratio of 1/8 is stable.

The relaxed geometry for the $(H_2)_{24}$/Eu_3/CNT system is shown in Fig. 8. Some regularity can be observed in the configurations while H_2 is adsorbed not only on Eu atoms (region 1), but also on CNT (region 2). Three H_2 molecules named "A", "B", and "C" are located at Atop, Bridge, and Hollow sites, respectively. The distances between H_2 and Eu have the sequence of C > A > B, which implies that H_{2C} (or H_{2B}) should have the weakest (or

strongest) binding in the three sites. In region 1, one Eu atom can adsorb up to five H_2. In region 2, H_{2C} moves to the center of the hexagonal ring and lies perpendicular to the tube. $E_{ad} = -0.09$ eV from GGA and -0.20 eV from LDA, exhibiting a physisorption. As Eu coverage reaches 1/8, 24 H_2 with $E_{ad} = -0.16$ eV/H_2 at GGA and -0.30 eV at LDA can be mostly adsorbed while DFT-GGA calculations usually underestimate E_{ad} and LDA calculations overestimate it [113, 114], The true E_{ad} could approach the lowest requirement of -0.20 eV/H_2 as proposed by the DOE. The corresponding hydrogen-storage capacity is 4.44 wt%.

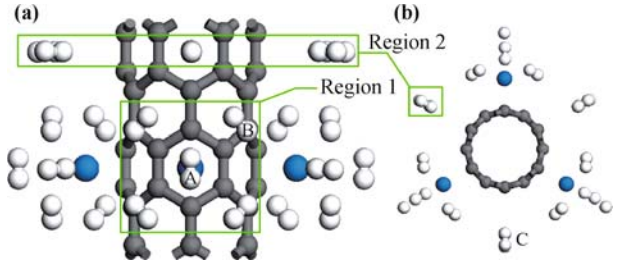

Fig. 8 Top view **(a)** and side view **(b)** for the optimized atomic structure of maximal number of adsorbed H_2 molecules for the Eu atoms doped CNT. The two insets show the fine views of Regions 1 and 2, which indicate the areas close to and far from the Eu atoms, respectively. Reproduced with permission from Ref. [35], Copyright © 2010 American Chemical Society.

Panels (a)–(e) in Fig. 9 illustrate the top views of the equilibrium configurations for the adsorption of one to five H_2 on the Eu/CNT system, respectively. When it is added onto the $(H_2)_5$/Eu/CNT system, the sixth H_2 moves away [see Fig. 9(f)]. Thus, at most five H_2 can be adsorbed around one Eu. E_{ad} slightly reduces from -0.26 to -0.22 eV/H_2 or from -0.49 to -0.40 eV/H_2 depending on GGA or LDA, respectively, which may result from the steric repulsion as n changes. Meanwhile the charge on Eu decreases with increased n, and the

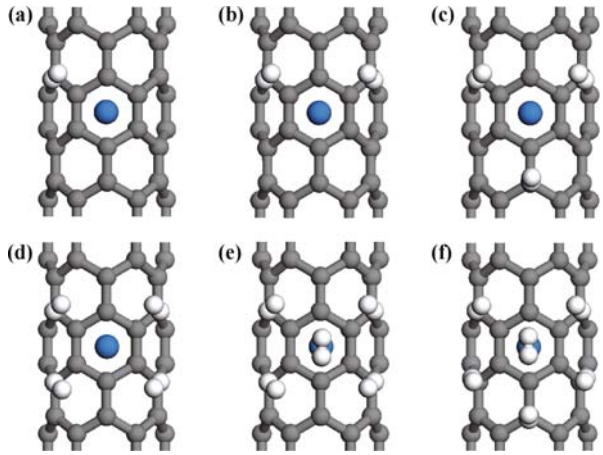

Fig. 9 The relaxed hydrogen storage systems based on H_2 adsorption on the Eu/CNT system with different numbers (n). The plots **(a)**–**(f)** show the optimized structures when n increases from 1 to 6. Reproduced with permission from Ref. [35], Copyright © 2010 American Chemical Society.

electric field around Eu also decreases. This, in turn, results in a distance drop between the adsorbed Eu and polarized H_2. The charge on CNT decreases as well. A single Eu on CNT can adsorb up to five H_2 molecules with $E_{ad} \sim -0.22$ eV/H_2 at GGA and -0.40 eV/H_2 at LDA, similar to the case of the Ca/CNT system [115]. These optimal E_{ad} values make hydrogen adsorption and desorption feasible at the ambient condition, which is critical for practical applications.

As a H_2 approaches Eu, Eu accepts electrons from H_2 while subsequently Eu transfers them to C atoms. This is indicated by the electronic configuration of Eu of $[Xe]4f^{6.991}5d^{0.732}6s^{0.250}6p^{0.130}$ in the H_2/Eu/CNT system. In the $(H_2)_5$/Eu/CNT system, the electronic configuration of Eu is $[Xe]4f^{6.969}5d^{0.928}6s^{0.309}6p^{0.296}$. Four other H_2 molecules thus add partial charge to Eu and occupy more orbitals of 5d and 6p subshells of Eu. Eu has difficulty donating electrons to H_2, but polarizes H_2 and binds them by electrostatic interaction. As more H_2 molecules are adsorbed, the Eu becomes less positively charged. The charge change on the Eu is cause by the electron donation from the dihydrogen bond to Eu. Consequently, the H–H bonds are elongated, and H_2 is mainly bound by the charge polarization mechanism with a small amount of electron transferred to Eu. This "insensitivity" in E_{ad} as a function of n is also a consequence of the mechanism that binds H_2, namely, the positive charge of the cation polarizes H_2, and the bonding results from an electrostatic interaction. Thus, the key to H_2 adsorption with binding energies at proper physisorbed states is to find a system where the positively charged state of metal atoms can remain. As n increases, Eu gets close to a limit state, which in turn reduces polarization.

The PDOS for $(H_2)_5$/Eu/CNT is shown in Fig. 10. The overlap of density state between H-1s orbital and Eu-4f, -5d, -6s, -6p orbitals appears at about 8 eV below the Fermi level E_F, where the hybridization takes place. This is especially evident between Eu-5d, Eu-6p and H-1s orbitals. There are three peaks between -9 and 0 eV in PDOS of Eu-5d orbital. The first two peaks around -0.5 and -2 eV correspond to the hybridization of Eu-5d and C-2p orbitals, which is responsible for the bonding of Eu and CNT. The third peak is related to the hybridization among Eu-5d, C-2p and H-1s orbitals. This suggests that Eu acts as a "bridge" in this reaction, in which it interacts with H_2 and CNT simultaneously. This result rationalizes the effect of Eu dopants on hydrogen storage. The PDOS of the Eu 4f orbital is much localized with a sharp peak. Thus, the electronic hybridization of Eu and H_2 orbitals leads to a partial H_2 adsorption to Eu/CNT apart from the electrostatic interaction. The former is always favorable to the binding, whereas the latter may change their roles in dependence on n. Although there are abundant half-filled Eu-4f orbitals, this Eu-4f band

exhibits a highly stable state, which brings about little electron transfer. As a result, Eu-4f electrons have little impact on the hybridization. It is expected that if the 4f orbital of doped RE elements is not empty, half-filled or full-filled, the 4f hybridization could begin.

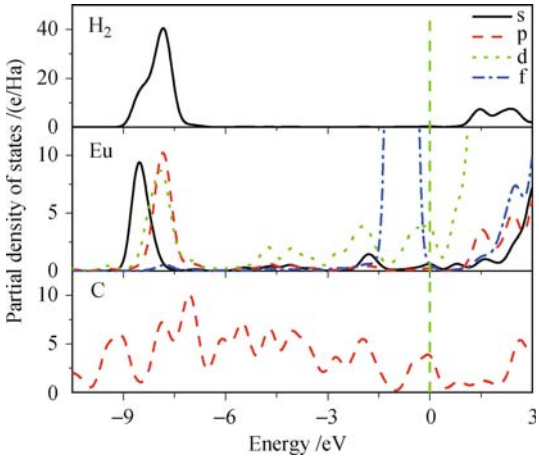

Fig. 10 The partial density of states (PDOS) plots for C atoms, Eu atom, and H_2 molecules of the $(H_2)_5$/Eu/CNT system in Fig. 9(e). The Fermi level is set to zero and indicated by a dotted line. Reproduced with permission from Ref. [35], Copyright © 2010 American Chemical Society.

6 Summary and prospects

As described above, several strategies for making advanced hydrogen storage materials have been developed, such as metal doping and external electrical field. The electric field is extremely important for hydrogen storage systems. The electric field induced structure variations, binding and hydrogen properties in metals-doped carbon nanostructures systems are reviewed. It is well known that metal atoms are decorated on carbon nanostructures to enhance their storage capacity. In addition, external electric fields have been proven to be an effective tool for redistributing charges, and thus some novel results can be achieved by superimposing a field into a system. The main conclusions are as follows:

1) Using an 8-Li-doped CNT, it is found that H_2 binding can be externally enhanced (or weakened) via superimposition of a positive (or negative) electric field. The calculated $E_{ad} = -0.58$ eV/H_2 under F=+0.010 a. u. is 93.33% lower than that under 0.000 a. u.. This is because the positive field produces an extra dipole moment. In contrast, E_{ad} increases from -0.30 to -0.20 eV/H_2 when F=−0.010 a. u.. In view of the fact that storage systems are insensitive to small unexpected field fluctuations, the application of the electric field as a reversible switch makes practical sense. Similar results can also be found in the Li-doped single-layer and bilayer graphenes. The results show that the binding strength increases by 88% when a field with a magnitude of +0.020 a.u. is imposed. Hirshfeld charge analysis results suggest that an increase in the binding strength will occur as long as the Li (or C) carries more positive (or negative) charges.

2) A high-capacity hydrogen storage medium–Al-adsorbed graphene–is proposed based on DFT calculations. It is found that a graphene layer with Al adsorbed on both sides can store hydrogen up to 13.79 wt% with average $E_{ad} = -0.193$ eV/H_2. Its HSC is in excess of 6 wt%, surpassing DOE's target. Based on the binding energy criterion and molecular dynamics calculations, the hydrogen storage system can be recycled at near ambient conditions. This high-capacity hydrogen storage is due to the adsorbed Al atoms that act as bridges to link the electron clouds of the H_2 molecules and the graphene layer. As a consequence, a two-layer arrangement of H_2 molecules is formed on each side of the Al adsorbed graphene layer. The H_2 concentration in the hydrogen storage medium can be measured by the change in the conductivity of the graphene layer.

3) The clustering tendency of TM is suppressed on boron-doped or defective carbon-base materials, which can thus be used as promising systems for hydrogen storage.

4) For the Eu/CNT system, the hollow site on the outer wall of CNT is the most favorable for the adsorption. The charge analysis results show that two 6s electrons in Eu transfer to CNT while 4f electrons remain in Eu, and the Eu atom is thus divalent. The results indicate that five H_2 per Eu atom can be adsorbed in the Eu/CNT system while 4.44 wt% H_2 can be stored in the Eu_3/CNT system. The interaction between H_2 and Eu/CNT is balanced by the electronic hybridization and electrostatic interactions.

In spite of favorable perspectives, there is still a lot of work to be done–especially the HSC of long-term cyclic stability tests–until the practicability of metal doped carbon nanostructures as hydrogen storage materials is proved or disproved. More correct calculations are needed where hydrogen desorption processes and metal clustering tendency need to be systematically considered now that hydrogen desorption processes are neglected in the above model. Hydrogen storage systems can not only adsorb up to 6 wt% of hydrogen but are also well capable of showing some interesting desorption. However, extensive work has not yet been done on desorption kinetics of metal-doped carbon nanostructures. In addition, metal clustering tendency must be overcome to maintain a high storage capacity of hydrogen at a stable level during hydrogen adsorption and desorption processes. It is therefore perhaps premature to discuss their possible applications, although their possible use as hydrogen energy sources with relatively high gravimetric and volumetric density, as required for instance for fuel cells, is obvious. Thus, research toward the application of metal doped carbon-based materials has just begun. Many challenges and opportunities remain.

Acknowledgements We acknowledge supports from the National Key Basic Research and Development Program of China (Grant No. 2010CB631001), the Program for Changjiang Scholars and Innovative Research Team in University, and High Performance Computing Center (HPCC) of Jilin University for supercomputer time.

References

1. S. A. Shevlin and Z. X. Guo, Chem. Soc. Rev., 2009, 28(1): 211
2. A. Züttel, Mater. Today, 2003, 6(9): 24
3. R. Coontz and R. Hanson, Science, 2004, 305(5686): 957
4. A. Züttel and S. Orimo, MRS Bull., 2002, 27(9): 705
5. S. Banerjee, S. Murad, and I. K. Puri, Proc. IEEE, 2006, 94(10): 1806
6. Q. Sun, P. Jena, Q. Wang, and M. J. Marquez, J. Am. Chem. Soc., 2006, 128(30): 9741
7. J. F. Stampfer, C. E. Holley, and J. F. Suttle, J. Am. Chem. Soc., 1960, 82(14): 3504
8. S. H. Jhi, Phys. Rev. B, 2006, 74(15): 155424
9. G. E. Froudakis, Nano Lett., 2001, 1(10): 531
10. I. Cabria, M. J. López, and J. A. Alonso, J. Chem. Phys., 2005, 123(20): 204721
11. S. H. Jhi, Catal. Today, 2007, 120(3–4): 383
12. X. J. Wu, Y. Gao, and X. C. Zeng, J. Phys. Chem. C, 2008, 112(22): 8458
13. L. Chen, Y. Zhang, N. Koratkar, P. Jena, and S. K. Nayak, Phys. Rev. B, 2008, 77(3): 033405
14. C. Liu, Y. Y. Fan, M. Liu, H. T. Cong, H. M. Cheng, and M. S. Dresselhaus, Science, 1999, 286(5442): 1127
15. O. V. Pupysheva, A. A. Farajian, and B. I. Yakobson, Nano Lett., 2008, 8(3): 767
16. K. R. S. Chandrakumar and S. K. Ghosh, Nano Lett., 2008, 8(1): 13
17. M. I. Rojas and E. P. M. Leiva, Phys. Rev. B, 2007, 76(15): 155415
18. J. B. Oostinga, H. B. Heersche, X. L. Liu, A. F. Morpurgo, and L. M. K. Vandersypen, Nat. Mater., 2008, 7(2): 151
19. A. K. Geim and K. S. Novoselov, Nat. Mater., 2007, 6(3): 183
20. A. Lherbier, X. Blase, Y. M. Niquet, F. Triozon, and S. Roche, Phys. Rev. Lett., 2008, 101(3): 036808
21. L. Schlapbach and A. Züttel, Nature, 2001, 414(6861): 353
22. K. S. Novoselov, A. K. Geim, S. V. Morozov, D. Jiang, Y. Zhang, S. V. Dubonos, I. V. Grigorieva, and A. A. Firsov, Science, 2004, 306(5696): 666
23. S. Patchkovskii, J. S. Tse, S. N. Yurchenko, L. Zhechkov, T. Heine, and G. Seifert, Proc. Natl. Acad. Sci. USA, 2005, 102(30): 10439
24. E. Durgun, S. Ciraci, and T. Yildirim, Phys. Rev. B, 2008, 77(8): 085405
25. T. Roman, W. A. Dino, H. Nakanishi, H. Kasai, T. Sugimoto, and K. Tange, Carbon, 2007, 45(1): 218
26. D. Li, M. B. Müller, S. Gilje, R. B. Kaner, and G. G. Wallace, Nat. Nanotechnol., 2008, 3(2): 101
27. C. Lee, X. Wei, J. W. Kysar, and J. Hone, Science, 2008, 321(5887): 385
28. U. Sahaym and M. G. Norton, J. Mater. Sci., 2008, 43(16): 5395
29. S. Orimo, A. Züttel, L. Schlapbach, G. Majer, T. Fukunaga, and H. Fujii, J. Alloys Comp., 2003, 356: 716
30. W. Liu, Y. H. Zhao, Y. Li, Q. Jiang, and E. J. Lavernia, J. Phys. Chem. C, 2009, 113(5): 2028
31. E. Klontzas, A. Mavrandonakis, E. Tylianakis, and G. E. Froudakis, Nano Lett., 2008, 8(6): 1572
32. W. Q. Deng, X. Xu, and W. A. Goddard, Phys. Rev. Lett., 2004, 92(16): 166103
33. E. Durgun, S. Ciraci, W. Zhou, and T. Yildirim, Phys. Rev. Lett., 2006, 97(22): 226102
34. Z. M. Ao and F. M. Peeters, Phys. Rev. B, 2010, 81(20): 205406
35. Z. W. Zhang, J. C. Li, and Q. Jiang, J. Phys. Chem. C, 2010, 114(17): 7733
36. G. Mpourmpakis, E. Tylianakis, and G. E. Froudakis, Nano Lett., 2007, 7(7): 1893
37. A. Nikitin, X. Li, Z. Zhang, H. Ogasawara, H. Dai, and A. Nilsson, Nano Lett., 2008, 8(1): 162
38. C. Ataca, E. Akturk, S. Ciraci, and H. Ustunel, Appl. Phys. Lett., 2008, 93(4): 043123
39. Z. M. Ao, Q. Jiang, R. Q. Zhang, T. T. Tan, and S. Li, J. Appl. Phys., 2009, 105(7): 074307
40. P. Chen, X. Wu, J. Lin, and K. L. Tan, Science, 1999, 285(5424): 91
41. R. T. Yang, Carbon, 2000, 38(4): 623
42. F. E. Pinkerton, B. G. Wicke, C. H. Olk, G. G. Tibbetts, G. P. Meisner, M. S. Meyer, and J. F. Herbst, J. Phys. Chem. B, 2000, 104(40): 9460
43. T. Yildirim and S. Ciraci, Phys. Rev. Lett., 2005, 94(17): 175501
44. Z. Zhou, J. J. Zhao, X. P. Gao, Z. F. Chen, J. Yan, P. R. Schleyer, and M. Morinaga, Chem. Mater., 2005, 17(5): 992
45. S. Dag, Y. Ozturk, S. Ciraci, and T. Yildirim, Phys. Rev. B, 2005, 72(15): 155404
46. J. W. Lee, H. S. Kim, J. Y. Lee, and J. K. Kang, Appl. Phys. Lett., 2006, 88(14): 143126
47. Q. Sun, Q. Wang, P. Jena, and Y. Kawazoe, J. Am. Chem. Soc., 2005, 127(42): 14582
48. B. Huang, H. Lee, W. Duan, and J. Ihm, Appl. Phys. Lett., 2008, 93(6): 063107
49. S. S. Han and A. William, J. Am. Chem. Soc., 2007, 129(27): 8422
50. K. L. Mulfort and J. T. J. Hupp, J. Am. Chem. Soc., 2007, 129(31): 9604
51. D. Zhao, D. Yuan, and H. C. Zhou, Energy & Environ. Sci., 2008, 1: 222
52. E. Klontazas, A. Mavrandonakis, E. Tylianakis, and G. E. Froudakis, Nano Lett., 2008, 8(6): 1572
53. X. Li, A. Grubisic, S. T. Stokes, J. Cordes, G. F. Ganteför, K. H. Bowen, B. Kiran, M. Willis, P. Jena, R. Burgert, and H. Schnöckel, Science, 2007, 315(5810): 356
54. C. Cento, P. Gislon, M. Bilgili, A. Masci, Q. Zheng, and P. P. Prosini, J. Alloys Comp., 2007, 437(1–2): 360
55. A. L. L. Dehouche, N. Grimard, J. Goyette, and R. Chahine, Nanotechnology, 2005, 16(4): 402
56. P. A. Berseth, A. G. Harter, R. Zidan, A. Blomqvist, C. M. Araújo, R. H. Scheicher, R. Ahuja, and P. Jena, Nano Lett., 2009, 9(4): 1501

57. C. H. Ahn, A. Bhattacharya, M. Di Ventra, J. N. Eckstein, C. D. Frisbie, M. E. Gershenson, A. M. Goldman, I. H. Inoue, J. Mannhart, D. Natelson, and J. M. Triscone, Rev. Mod. Phys., 2006, 78(4): 1185
58. L. Qiao, W. T. Zheng, Q. B. Wen, and Q. Jiang, Nanotechnology, 2007, 18(15): 155707
59. M. Tomonari and O. Sugino, Chem. Phys. Lett., 2007, 437(4-6): 170
60. A. Migani, C. Sousa, F. Sanz, and F. Illas, Phys. Chem. Chem. Phys., 2005, 7(18): 3353
61. T. Ohta, A. Bostwick, T. Seyller, K. Horn, and E. Rotenberg, Science, 2006, 313(5789): 951
62. S. Zou and M. Weaver, J. Phys. Chem., 1996, 100(10): 4237
63. S. Zou and M. Weaver, Anal. Chem., 1998, 70(11): 2387
64. E. V. Castro, K. S. Novoselov, S. V. Morozov, N. M. R. Peres, J. M. dos Santos, J. Nilsson, F. Guinea, A. K. Geim, and A. H. C. Neto, Phys. Rev. Lett., 2007, 99(21): 216802
65. R. Q. Zhang, W. T. Zheng, and Q. Jiang, J. Phys. Chem. C, 2009, 113(24): 10384
66. W. Liu, Y. H. Zhao, Y. Li, E. J. Lavernia, and Q. Jiang, Phys. Chem. Chem. Phys., 2009, 11(40): 9233
67. W. Liu, Y. H. Zhao, J. Nguyen, Y. Li, Q. Jiang, and E. J. Lavernia, Carbon, 2009, 47(15): 3452
68. Z. M. Ao, W. T. Zheng, and Q. Jiang, Nanotechnology, 2008, 19(27): 275710
69. J. Zhou, Q. Wang, Q. Sun, P. Jena, and X. S. Chen, Proc. Natl. Acad. Sci. USA, 2010, 107(7): 2801
70. S. Gemming, T. Kunze, K. Morawetz, V. Pankoke, R. Luschtinetz, and G. Seifert, Eur. Phys. J. Spec. Top., 2009, 177(1): 83
71. H. Gronbeck, Top. Catal., 2004, 28(1-4): 59
72. P. Hohenberg and W. Kohn, Phys. Rev. B, 1964, 136: B864
73. G. Kresse and J. Fürthmuller, Comput. Mater. Sci., 1996, 6(1): 15
74. B. Delley, J. Chem. Phys., 1990, 92(1): 508
75. M. D. Segall, P. J. D. Lindan, M. J. Probert, C. J. Pickard, P. J. Hasnip, S. J. Clark, and M. C. Payne, J. Phys.: Condens. Matter, 2002, 14(11): 2717
76. The help of the Materials Studio Modeling
77. B. Delley, J. Chem. Phys., 2000, 113(18): 7756
78. B. K. Rao and P. Jena, Europhys. Lett., 1992, 20(4): 307
79. M. Y. Ni, L. F. Huang, L. J. Guo, and Z. Zeng, Int. J. Hydrogen Energy, 2010, 35(8): 3546
80. A. Tokura, F. Maeda, Y. Teraoka, A. Yoshigoe, D. Takagi, Y. Homma, Y. Watanabe, and Y. Kobayashi, Carbon, 2008, 46(14): 1903
81. G. Y. Zhang, P. F. Qi, X. R. Wang, Y. R. Lu, D. Mann, X. L. Li, and H. J. Dai, J. Am. Chem. Soc., 2006, 128(18): 6026
82. B. Panella, K. Hones, U. Muller, N. Trukhan, M. Schubert, H. Putter, and M. Hirscher, Angew. Chem. Int. Ed., 2008, 47(11): 2138
83. A. F. Vilaplana, J. Phys. Chem. C, 2008, 112(10): 3998
84. D. Henwood and J. D. Carey, Phys. Rev. B, 2007, 75(24): 245413
85. J. S. Arellano, L. M. Molina, A. Rubio, and J. A. Alonso, J. Chem. Phys., 2000, 112(18): 8114
86. G. K. Dimitrakakis, E. Tylianakis, and G. E. Froudakis, Nano Lett., 2008, 8(10): 3166
87. M. Aertsens and J. Naudts, J. Stat. Phys., 1991, 62(3–4): 609
88. J. Graetz, S. Chaudhuri, Y. Lee, T. Vogt, J. T. Muckerman, and J. J. Reilly, Phys. Rev. B, 2006, 74(21): 214114
89. J. Li, T. Furuta, H. Goto, T. Ohashi, Y. Fujiwara, and S. Yip, J. Chem. Phys., 2003, 119(4): 2376
90. F. Schedin, A. K. Geim, S. V. Morozov, E. W. Hill, P. Blake, M. I. Katsnelson, and K. S. Novoselov, Nat. Mater., 2007, 6(9): 652
91. C. He, P. Zhang, Y. F. Zhu, and Q. Jiang, J. Phys. Chem. C, 2008, 112(24): 9045
92. Y. F. Zhao, Y. H. Kim, A. C. Dillon, M. J. Heben, and S. B. Zhang, Phys. Rev. Lett., 2005, 94: 155504
93. E. Durgun, Y. R. Jang, and S. Ciraci, Phys. Rev. B, 2007, 76(7): 073413
94. H. Lee, W. I. Choi, and J. Ihm, Phys. Rev. Lett., 2006, 97(5): 056104
95. G. Kim, S. H. Jhi, N. Park, S. G. Louie, and M. L. Cohen, Phys. Rev. B, 2008, 78(8): 085408
96. G. Kim, S. H. Jhi, and N. Park, Appl. Phys. Lett., 2008, 92(1): 013106
97. S. A. Shevlin and Z. X. Guo, J. Phys. Chem. C, 2008, 112(44): 17456
98. S. Meng, E. Kaxiras, and Z. Zhang, Nano Lett., 2007, 7(3): 663
99. G. J. Kubas, R. R. Ryan, B. I. Swanson, P. J. Vergamini, and H. J. Wasserman, J. Am. Chem. Soc., 1984, 106(2): 451
100. S. Barman, P. Sen, and G. P. Das, J. Phys. Chem. C, 2008, 112(50): 19963
101. G. J. Kubas, Acc. Chem. Res., 1988, 21(3): 120
102. J. Niu, B. K. Rao, and P. Jena, Phys. Rev. Lett., 1992, 68(15): 2277
103. M. Yoon, S. Y. Yang, C. Hicke, E. Wang, D. Geohegan, and Z. Y. Zhang, Phys. Rev. Lett., 2008, 100(20): 206806
104. Q. Sun, Q. Wang, and P. Jena, Appl. Phys. Lett., 2009, 94(1): 013111
105. A. Bhattacharya, S. Bhattacharya, C. Majumder, and G. P. Das, J. Phys. Chem. C, 2010, 114(22): 10297
106. Y. G. Zhou, X. T. Zu, F. Gao, J. L. Nie, and H. Y. Xiao, J. Appl. Phys., 2009, 105(1): 14309
107. L. Firlej, B. Kuchta, C. Wexler, and P. Pfeifer, Adsorption, 2009, 15(3): 312
108. H. L. Park and Y. C. Chung, Comput. Mater. Sci., 2010, 49(4): S297
109. S. Suzuki, M. Kushida, S. Amamiya, S. Okada, and K. Nakao, Chem. Phys. Lett., 2000, 327(5–6): 291
110. G. L. Lu, K. M. Deng, H. P. Wu, J. L. Yang, and X. Wang, J. Chem. Phys., 2006, 124(5): 054305
111. X. X. Wang, X. Y. Li, and H. N. Li, Phys. Lett. A, 2008, 372(44): 6677
112. B. Delley, Phys. Rev. B, 2002, 66(15): 155125
113. Y. H. Kim, Y. F. Zhao, A. Williamson, M. J. Heben, and S. B. Zhang, Phys. Rev. Lett., 2006, 96(1): 016102
114. Y. Gao and X. C. Zeng, J. Phys.: Condens. Matter, 2007, 19(38): 386220
115. X. B. Yang, R. Q. Zhang, and J. Ni, Phys. Rev. B, 2009, 79(7): 075431